ACS APPLIED MATERIALS & INTERFACES

Research Article

Cite This: ACS Appl. Mater. Interfaces 2018, 10, 32510−32515

www.acsami.org

Protecting Ceria Nanocatalysts—The Role of Sacrificial Barriers

Lucy M. Morgan,*[,†] Marco Molinari,[‡] Anna Corrias,[†] and Dean C. Sayle*[,†]

[†]School of Physical Sciences, University of Kent, Canterbury CT2 7NH, U.K.

[‡]Department of Chemistry, University of Huddersfield, Huddersfield HD1 3DH, U.K.

Supporting Information

ABSTRACT: Forces acting on a functional nanomaterial during operation can cause plastic deformation and extinguish desirable catalytic activities. Here, we show that sacrificial materials, introduced into the catalytic composite device, can absorb some of the imposed stress and protect the structural integrity and hence the activity of the functional component. Specifically, we use molecular dynamics to simulate uniaxial stress on a ceria (CeO_2) nanocube, an important functional material with respect to oxidative catalysis, such as the conversion of CO to CO_2. We predict that the nanocube, protected by a "soft" BaO or "hard" MgO sacrificial barrier, is able to withstand 40.1 or 26.5 GPa, respectively, before plastic deformation destroys the structure irreversibly; the sacrificial materials, BaO and MgO, capture 71 and 54% of the stress, respectively. In comparison, the unprotected nanoceria catalyst deforms plastically at only 2.5 GPa. Furthermore, modeling reveals the deformation mechanisms and the importance of microstructural features, insights that are difficult to measure experimentally.

KEYWORDS: *molecular dynamics, catalytic reactivity, mechanical properties, ceria nanocubes, stress−strain curves, nanomaterials*

INTRODUCTION

The properties of a functional material can be tuned by changing its size and shape (metamaterial sculpting) as an alternative to elemental control.[1] It is therefore not surprising that the properties of functional materials are being revisited as a function of nanostructuring, as evidenced, in part, by the creation of 70 new journals devoted to nanoscience.[2] However, the consequence of traversing to the nanoscale can be severe. For example, small forces can translate to considerable pressures when contact areas are reduced to the nanoscale. In particular, when the same force acts upon a contact area that is reduced from 1 cm^2 to 10 nm^2, the pressure increases by 13 orders of magnitude. Plastic deformation of a nanomaterial will irreversibly extinguish any desirable properties; therefore, it is vital to understand the mechanical properties of functional nanomaterials. For example, Huang et al. showed that the intercalation of Li into SnO_2 nanowires introduced considerable localized stress. This resulted in plastic deformation and pulverization of the material; such major mechanical effects plague the performance and lifetime of high-capacity anodes in lithium-ion batteries.[3]

A catalytically important functional nanomaterial, ceria, CeO_2, has been the subject of intense scrutiny because of its remarkable properties, including surface activity,[4] redox and defect chemistry,[5] oxygen transport[6] with application for energy materials (including solid oxide fuel cells),[7] catalysis,[8] nanomedicine,[9] and chemical mechanical planarization.[10,11] For example, ceria, in nanoform, has been shown to be a highly active catalyst; CeO_2 nanocubes can catalyze CO to CO_2 at room temperature in contrast to the parent bulk material.[12] Currently, ceria is used as a component of three-way automobile exhaust catalysts,[13] and if ceria is to be replaced by its nanostructured counterpart, it must resist damage under the harsh environmental conditions associated with its operation, such as extremes of temperature, impact, friction, and wear.

Current composite catalysts include features such as expanding mats and enclosures to protect the active material in working conditions.[14] The design of the composite catalyst can therefore be informed by considering the sacrificial ability of some of the component materials of the composite catalyst.

An additional consideration is that many nanosystems are composed of multiple nanomaterials, for example, nanocomposites. Here, it is important to understand not only how each component responds individually to stress but also in combination. For example, if stress is imposed upon a core−shell system, how does the system partition the stress? Does the shell accommodate some of the strain and then impose the residual stress upon the inner core? If the shell is "harder" than the core, would the partition of stress be different to the reverse? Such an understanding will reveal insight into "sacrificial" and protective nanomaterials.

Stress can originate from a variety of sources in addition to mechanical load, operational vibration, or friction. For example, the differences in the thermal expansion coefficients of two interfaced materials will induce stress when a system is exposed to high-temperature fluctuations. Similarly, intercalation and substitution cause localized lattice expansion that will impart stress on neighboring regions that have not (yet) intercalated an ion.[15]

Received: May 26, 2018
Accepted: August 30, 2018
Published: August 30, 2018

Some insight into this area is already available. In particular, during the mechanical testing of nanomaterials, the anvils, used to communicate pressure upon the test material, will likely themselves deform;[16] a soft anvil, such as a metal, will likely suffer greater deformation than a hard anvil, such as diamond.[17] Accordingly, we question how anvil hardness influences the catalytic and mechanical properties and deformation behavior of a material measured using such anvils. The relationships between the mechanical properties and nanostructure have been investigated experimentally using nanoindentation,[18] transmission electron microscopy (TEM),[19] and atomic force microscopy.[20] Characterizing the structural changes and time-resolved stress−strain properties is challenging experimentally.[21] Computer simulation can therefore play a key complementary role to gain insight into these changes at the atomistic level and track their progress.

Notwithstanding its remarkable properties and diverse range of applications, there is limited information pertaining to the mechanical properties of nanoceria reported in the open literature. This does not mean that the mechanical strength of nanoceria has gone entirely unconsidered, though the research is not always in agreement. For example, simulating uniaxial force, Caddeo et al.[22] determined a yield strength of 12 GPa at 0.20 strain for a ceria nanocube. In contrast, also using simulated uniaxial force, cubic nanoporous ceria reported by Sayle et al. determined a yield strength range of 5.4−13.8 GPa at 0.06−0.08 strain, dependent on the axial direction.[23] Although the reported yield strengths are of a similar magnitude, the strain of the porous material is less than half that of the nanocube. Comparatively, the bulk material, measured via density functional theory (DFT) was reported by Sakanoi et al. to have a yield strength of 22.7 GPa at 0.09 strain.[24]

The influence of the anvil structure such as the surface roughness[25] and indenter shape[26] has been investigated and shown to influence the measured strength of the subject material. This highlights the importance of including shape and surface defects in computational simulations. If a material contains surface steps and deformations, it will have an impact on the measured hardness.

Here, we simulate a ceria nanocube under compression between fixed and deformable anvils and use MgO and BaO as systems representative of hard and soft anvils, respectively. We explore the deformation within the nanoceria test material and deformation suffered by the anvils, as well as the effect this may have on the catalytic activity.

METHODS

Potential Models. All simulations are based on the Born model of the ionic solid. The energy of the system is given by

$$E(r_{ij}) = \sum_{ij} \frac{Q_i Q_j}{4\pi\varepsilon_0 r_{ij}} + \sum_{ij} A \exp\left(\frac{-r_{ij}}{\rho}\right) - C r_{ij}^{-6} \quad (1)$$

where the first term represents the Coulombic interaction between ions, i and j, of charges Q_i and Q_j, respectively, at a distance of r_{ij}. The second and third terms represent the Buckingham form with the potential values[22,27] presented in Table 1. All cation−cation interactions were set to zero.

Building Atomistic Models. Simulated amorphization and recrystallization[28] was used to generate atom-level models of the anvils. This technique, analogous to experiment, enables microstructural features to evolve during the crystallization step. The structural models are therefore more realistic in that they capture structural features observed experimentally. These include surface steps, vacancies (Figure 1), interstitials, dislocations, and grain-boundaries. This is important because the mechanical properties of a material are governed by its microstructure.[29]

Table 1. Buckingham Potential Parameters Used in the Molecular Dynamic Simulations

atom i	atom j	A/eV	ρ/Å	C/eV Å^{-6}
Ce^{4+}	O^{2-}	1986.83	0.3511	20.40
Mg^{2+}	O^{2-}	1428.50	0.2945	0.00
Ba^{2+}	O^{2-}	931.70	0.3939	0.00
O^{2-}	O^{2-}	22 764.00	0.1494	27.88

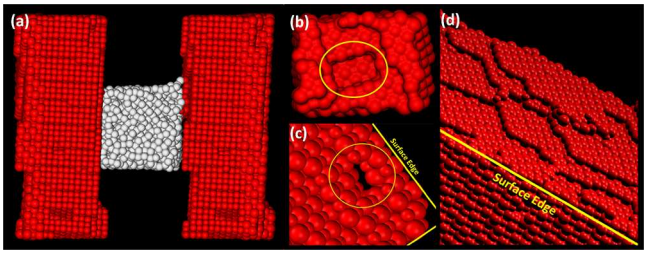

Figure 1. (a) Image showing the ceria nanoparticle, colored white, sandwiched between two anvils, colored red. The structural complexity of the anvil can be seen in (b), (c), and (d). (b) shows a void on the surface of the anvil, (c) shows a void along the edge of the anvil, and (d) shows a variety of steps on the anvil surface.

The atomistic structure of the model ceria nanocube comprises six {100} surfaces, with extensive surface relaxation along the edges in accord with the real nanomaterial.[30] The atomistic structures for the MgO and BaO anvils comprise {100} surfaces with a variety of steps and edged stepped {100} surfaces, in accord with the real materials.[31] Further details are given in the Supporting Information.

Elastic Constants. The elastic constants of the MgO and BaO anvils were calculated with the GULP code,[32] using potential parameters reported in Table 1.

Uniaxial Compression. Uniaxial compression was performed under constant volume (NVT) molecular dynamics (MD) simulation.[33] The atoms at the back of one anvil were then moved by 0.02 Å every 100 steps (step size 0.002 ps) to give a compression rate of 0.1 Å ps^{-1} (10 ms^{-1}). The strain within the system is expressed as

$$\varepsilon = \frac{(L_i - L_n)}{L_i} \quad (2)$$

where ϵ is the strain, L_i is the initial distance between the anvils, and L_n is the distance after each 100 steps of the compression (each movement of the anvil). As only uniaxial compression is considered, the strains are reported as positive values between 0 and 1.

Structural Analysis. Molecular graphics analysis and visualization was performed using VMD[34] and Materials Studio.

Stress Partitioning. During the compressions, the total imposed stress is partitioned between the anvils and the ceria nanocube. It is therefore important to deconvolute the total stress to reveal how much stress is captured by the anvils and the subsequent residual stress imposed upon the nanoceria. We describe how we calculated these values in the Supporting Information.

RESULTS

Stress−Strain Relationship. The stress−strain curves for the ceria nanocube using nondeformable (fixed), hard (MgO), and soft (BaO) anvils are shown in Figure 2. These figures show the total stress (black), the stress absorbed by the anvils (gray), and the residual stress acting upon the ceria nanocube (orange/green/blue). Details of the highlighted events

DOI: 10.1021/acsami.8b08674
ACS Appl. Mater. Interfaces 2018, 10, 32510−32515

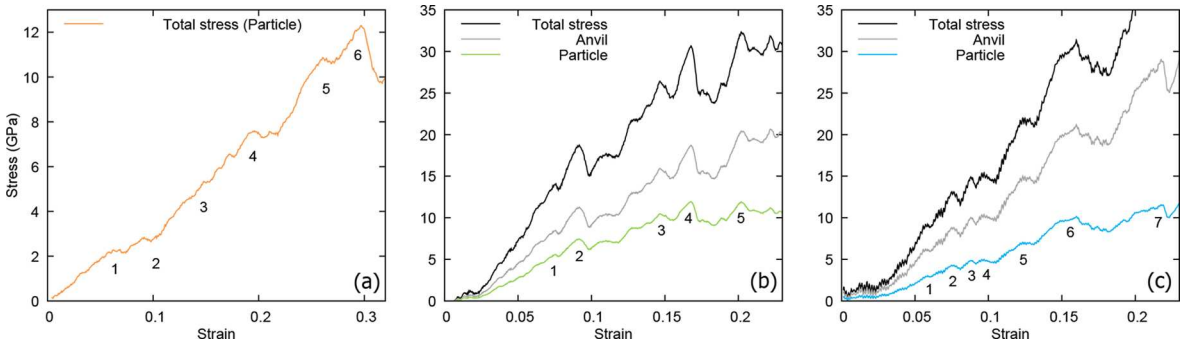

Figure 2. Stress−strain curves of nanoceria using: (a) fixed anvils, (b) MgO anvils, and (c) BaO anvils. In each stress−strain curve, the total stress (black), stress on anvil (gray), and residual stress on nanoceria sample (orange/green/blue) are given. The numbers correspond to the data points highlighted in Table 2 and represent significant events during the deformation process.

Table 2. Details Describing Events during the Deformation of the Nanocube, at the Locations Given in Figure 2, as Observed through Visual Analysis[a]

	fixed anvils		hard anvils (MgO)		soft anvils (BaO)	
	strain, stress	deformation event	strain, stress	deformation event	strain, stress	deformation event
1	0.06, 2.2	twist (particle)	0.07, 5.6	particle (minor)	0.06, 2.8	anvil, anvil
2	**0.10, 2.5**	**particle (moderate)**	0.09, 7.4	anvil and particle (minor)	0.08, 4.2	anvil, anvil
3	0.15, 5.0	particle (moderate)	0.15, 10.6	anvil and particle (minor)	0.09, 4.9	particle (minor)
4	0.20, 7.8	particle (moderate)	**0.17, 12.1**	**particle (minor)**	0.095, 5.0	particle corner (minor)
5	0.26, 10.7	particle (moderate)	0.21, 12.1	particle (major)	0.12, 7.2	particle rotates slightly
6	0.30, 12.4	particle (moderate)			0.16, 10.0	anvil and particle (minor)
7					**0.22, 11.6**	**particle (major)**

[a]Stress values are reported in GPa; emphasized data (bold font) relates to the yield point. Further details given in Supporting Information.

(numbered on the graphs) are presented in Table 2, with larger figures, and further details given in the Supporting Information. The yield strength was determined when both of the following criteria were satisfied: sudden system stress release (drop in the stress−strain curve) and a corresponding plastic deformation event in the *ceria nanoparticle*. In particular, there are several occurrences of sudden system stress release. However, these events correspond to the sacrificial material capturing the stress, via a plastic deformation event and not the nanoceria catalyst.

Experimentally, Young's modulus is based upon the total stress, without consideration of stress partitioning. Here, we report Young's modulus and yield strength calculated for the ceria nanocube using hard, soft, and fixed anvils, in Table 3. The yield strength, the first point of irreversible plastic deformation, is referred to as moderate/major deformation and was determined by visual analysis. This is seen as a point of discontinuity in the stress−strains (i.e., Figure 2b(2)). Minor deformations were considered potentially reversible through the removal of the anvils and extended equilibration time, for example Figure 2b(1).

Table 3. Mechanical Properties of a Ceria Nanocube, Calculated Using Soft, Hard, and Fixed Anvils[a]

	soft anvils (BaO)	hard anvils (MgO)	fixed anvils
yield strain	0.22	0.17	0.10
particle yield strength [%]	11.6 [29%]	12.1 [46%]	2.5 [100%]
anvil yield strength [%]	28.5 [71%]	14.4 [54%]	
total strength	40.1	26.5	2.5
anvil elastic constants, C_{11}, C_{12}	122, 58	393, 164	∞, ∞
Young's modulus (particle)	88	75	56

[a]Yield strength, total strength, elastic constants, and Young's modulus are reported in GPa. Percentage yield strength, [%], relates to the partitioning of the stress between the ceria nanoparticle and the anvil.

Structure and Radial Distribution Function. Nanoceria can catalyze an oxidation/reduction reaction by capturing, storing, and releasing oxygen.[35] The catalytic activity is dependent upon the surface(s) exposed. In particular, ceria {111} surfaces are thermodynamically more stable than {100} surfaces. On the other hand, it is energetically easier to extract oxygen from the {100} surfaces, and therefore, nanoceria, which exposes {100} surfaces is catalytically more active than nanoceria exposing {111}.

Our model ceria nanocube exposes six {100} surfaces, Figure 3, and therefore a key indicator of the catalytic activity is the structural preservation of the fluorite crystal structure and {100} surfaces under uniaxial loading. Figure 3 shows the structure of the ceria nanocube under 20% compression with BaO (soft), MgO (hard), and no sacrificial material for protection. Inspection of the model ceria nanocubes, using molecular graphics, reveals that the structural integrity of the {100} surfaces and fluorite crystal structure is retained when protected by BaO and partially retained with MgO. Conversely, with no sacrificial material, the nanocube deforms plastically, resulting in an almost amorphous particle, Figure 3 (orange).

The calculated radial distribution functions (RDFs) provide additional insight into the structural deformations and are shown in Figure 4. Inspection of the RDF reveal that when protected by BaO, the ceria nanocube retains long-range order. Specifically, the RDF trace is almost identical for the ceria nanocube under 0 and 20% strain, Figure 4 (blue). Conversely, when protected by MgO, the peaks start to broaden, Figure 4

DOI: 10.1021/acsami.8b08674
ACS Appl. Mater. Interfaces 2018, 10, 32510−32515

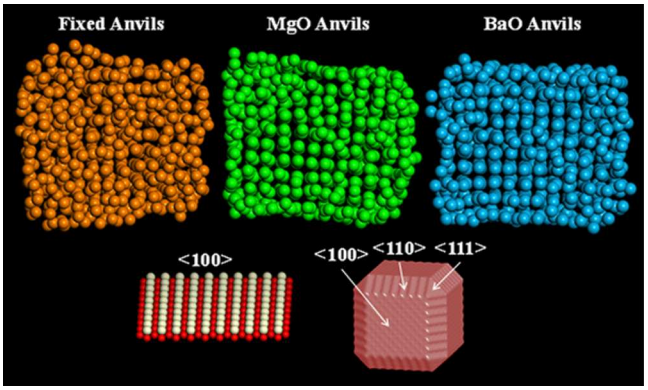

Figure 3. Cation structure of nanoceria at 20% compression using fixed anvils (top left), MgO anvils (top center), and BaO anvils (top right). Here, the loss of ordered structure can be seen in varying degrees, with fixed anvils suffering the most loss of structure and BaO the least. The atom-level structure of the perfect CeO_2 {100} surface and the morphology of the ceria nanocube is shown bottom left and bottom right, respectively.

(green), indicating some structural deformation. Unprotected, the long-range order is almost completely extinguished, Figure 4 (orange).

The atom-level structures and calculated RDFs are consistent with the calculated yield strain of each system, Figure 2, Table 2. At 20% strain, we expect almost complete loss of structural integrity for the unprotected ceria nanocube (yield strain 10% at 2.5 GPa), partial loss for the MgO-protected nanocube (yield strain 17% at 26.5 GPa), and minimal to no loss for the BaO-protected nanocube (yield strain 22% at 40 GPa) Figure 4.

We propose that BaO and MgO act "sacrificially", preserving the structure and hence catalytic activity of the nanoceria catalyst. The softer material (BaO) provides the greatest protection and can withstand uniaxial stresses of up to 40 GPa.

DISCUSSION

It is well known that anvil hardness affects measured stress, though not to what extent. Accordingly, (hard) diamond anvils are commonly used to ensure that the imposed stress is communicated almost completely to the sample. Conversely, measurements using more malleable anvils[16] may over-report the yield stress because of load partitioning. Our calculations reveal that the soft (BaO) anvil can capture as much as 71% of the imposed stress. As expected, the harder anvil captures less of the imposed stress—in this case, 54% (MgO anvil), Table 3. The use of soft anvils makes it possible to gain insight into protective or "sacrificial" materials. Here, stress partitioning is key to their performance. This is especially important for devices that comprise composite functional materials, such as batteries,[15] fuel cells,[7] chemical mechanical planarization slurries,[11] and catalysts.[8]

It might appear that stresses of GPa magnitude are unlikely during operating conditions. However, for nanomaterials, where surface areas can be of the order of tens of nm^2, localized regions can easily suffer such high levels of stress. Examples may include Li intercalation (charge cycling of batteries), friction,[36] impact,[37] and even temperature fluctuations[38] (relative expansion coefficients of composite nanomaterials). Caution must therefore be exercised in using documented information when designing devices that will be subject to high levels of operational stress.

Further to this, "real" materials contain microstructural features including differences in morphology, grain-boundary, dislocation, and point defect concentrations, which emanate from the synthetic protocol.[39] As mechanical properties are governed by its microstructure, measured values can therefore differ by orders of magnitude. For example, Sato et al. determined a fracture strength of 0.25 GPa, measured using Vickers indentation,[40] whereas Sakanoi et al.[24] calculated a fracture strength of 22.70 GPa for the same material using DFT.

More recently, microstructural features have been introduced into model structures, enabling more realistic simulations of mechanical properties.[22,23] By using a simulated amorphization and crystallization technique to generate the atom-level models, it enables microstructural features to evolve "naturally" within the model, analogous to their evolution during the crystallization step in synthesis.

The study of nanocompression, as opposed to indentation, is possible experimentally and is starting to gain interest among the nanomaterial community.[42] Recently, an in situ TEM study of multicycle rubbing of ceria nanoclusters was performed by Bhatta et al.[41] using a flat diamond probe. The study revealed plastic deformation of the nanoceria with evidence of fracture formation. In addition, Epicier et al.[43] explored how the oxidation state of ceria nanoparticles affects the mechanical properties; stress−strain curves revealed the pseudoelastic response of the material. Epicier also iterates the experimental challenges associated with in situ microstructural characterization and advocates the use of MD as a complementary tool,

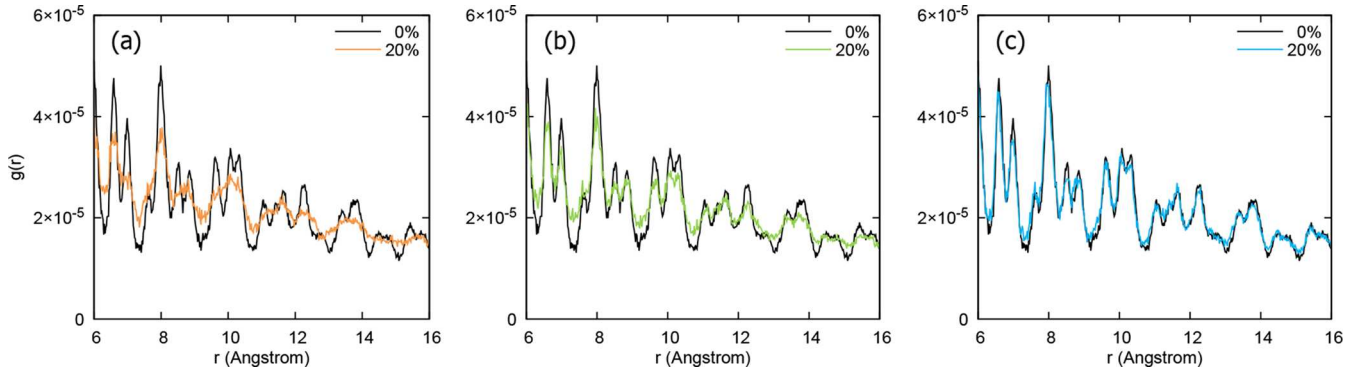

Figure 4. Radial Distribution Functions, RDF, within nanoceria using (a) fixed anvils, (b) MgO anvils, and (c) BaO anvils, at both 0 and 20% compression, highlighting the loss of long-range order.

DOI: 10.1021/acsami.8b08674
ACS Appl. Mater. Interfaces 2018, 10, 32510−32515

specifically, the capability of MD simulations to provide atom-level insight into areas such as stress-induced nucleation of dislocations, which emanate from the surface.

The Boussinesq problem relates to determining the elastic state in a linearly elastic isotropic half-space, which is subject to an applied load concentrated perpendicular to its boundary.[44] Elasticity therefore plays a vital role in contact mechanics,[45] and in recent years, nanoindentation has become fairly effective for measuring the mechanical properties, such as the elastic modulus and yield stress of nanomaterials.[46] These experimental techniques have time resolution in the order of microseconds or larger and may therefore not resolve all mechanical deformation events occurring within the material. Computational methods, such as MD, have nanosecond resolution enabling these subtle "stress-quenching" events to be captured at the atomic level, giving exceptional detail of the in situ mechanical deformation. Conversely, the time window accessible to MD simulations is normally microseconds or less, and therefore, the deformation rate is normally high. Accordingly, experiment and simulation together offer complementary insight.

CONCLUSIONS

We predict using MD simulation that deformable anvils can act as a protective barrier for catalytically active nanomaterials such as ceria. In particular, we use MD to simulate the deformation of a ceria nanocube sandwiched between soft BaO and hard MgO anvils and compare the results with deformation of the nanoceria when unprotected. We find that the nanoceria resists plastic deformation up to 40.1 GPa (BaO), 26.5 GPa (MgO), and 2.5 GPa (unprotected). Our simulations reveal that the soft anvils increase nanoparticle protection by absorbing more of the stress; the BaO and MgO anvils are able to capture 71 and 54% of the imposed stress, respectively.

Our simulations reveal the importance of considering deformable anvils, which include microstructural features, such as dislocations and surface roughening, when simulating stress-induced plastic deformation. In particular, the yield strength of nanoceria, measured as the residual stress acting upon the nanoparticle just before plastic deformation, was calculated to be 11.6 GPa (soft—BaO), 12.1 GPa (hard—MgO), and 2.5 GPa (no anvil).

Analysis of the structures reported in this study gives an indication of a change in the catalytic behavior of nanoceria under uniaxial stress, thereby affecting the activity of the functional material, with further evidence presenting the effects of a hostile environment on this behavior.

ASSOCIATED CONTENT

Supporting Information

The Supporting Information is available free of charge on the ACS Publications website at DOI: 10.1021/acsami.8b08674.

Further details relating to the atomistic models, stress partitioning, structure and catalysis, deformation mechanisms, RDFs, and stress-induced amorphization and evidence of oxygen exchange, deformation from surface steps, and more detailed depictions of deformation events (PDF)

Fixed anvils: ceria nanocube (white) compression by nondeformable anvils (orange) (ZIP)

MgO anvils: ceria nanocube (white) compression by hard anvils (green) (ZIP)

BaO anvils: ceria nanocube (white) compression by soft anvils (blue) (ZIP)

AUTHOR INFORMATION

Corresponding Authors

*E-mail: L.M.Morgan@kent.ac.uk (L.M.M.).

*E-mail: D.C.Sayle@kent.ac.uk (D.C.S.).

ORCID

Lucy M. Morgan: 0000-0002-6432-3760

Marco Molinari: 0000-0001-7144-6075

Anna Corrias: 0000-0002-5190-8196

Dean C. Sayle: 0000-0001-7227-9010

Notes

The authors declare no competing financial interest.

ACKNOWLEDGMENTS

The authors thank the Engineering and Physical Sciences Research Council (EPSRC), the School of Physical Sciences, University of Kent, Francesco Caddeo for valuable assistance and advice, and Agata Rożek for her computational assistance. We are grateful to the UK Materials and Molecular Modelling Hub for computational resources, which are partially funded by EPSRC (EP/P020194/1), and for funding by EP/1641783 and EP/R010366/1.

REFERENCES

(1) Li, Y.; Shen, W. Morphology-Dependent Nanocatalysts: Rod-Shaped Oxides. *Chem. Soc. Rev.* **2014**, *43*, 1543−1574.

(2) Rogach, A. How Many Nano Journals Does the World Need? *ACS Nano* **2012**, *6*, 9349.

(3) Huang, J. Y.; Zhong, L.; Wang, C. M.; Sullivan, J. P.; Xu, W.; Zhang, L. Q.; Mao, S. X.; Hudak, N. S.; Liu, X. H.; Subramanian, A.; Fan, H.; Qi, L.; Kushima, A.; Li, J. In Situ Observation of the Electrochemical Lithiation of a Single SnO_2 Nanowire Electrode$_2$ Nanowire Electrode. *Science* **2010**, *330*, 1515−1520.

(4) Zhou, K.; Wang, X.; Sun, X.; Peng, Q.; Li, Y. Enhanced Catalytic Activity of Ceria Nanorods from Well-Defined Reactive Crystal Planes. *J. Catal.* **2005**, *229*, 206−212.

(5) Mogensen, M.; Sammes, N.; Tompsett, G. Physical, Chemical and Electrochemical Properties of Pure and Doped ceria. *Solid State Ionics* **2000**, *129*, 63−94.

(6) Holmgren, A.; Duprez, D.; Andersson, B. A Model of Oxygen Transport in Pt/Ceria Catalysts from Isotope Exchange. *J. Catal.* **1999**, *182*, 441−448.

(7) Malavasi, L.; Fisher, C. A. J.; Islam, M. S. Oxide-ion and Proton Conducting Electrolyte Materials for Clean Energy applications: structural and mechanistic features. *Chem. Soc. Rev.* **2010**, *39*, 4370−4387.

(8) Ta, N.; Liu, J.; Shen, W. Tuning the Shape of Ceria Nanomaterials for Catalytic Applications. *Chin. J. Catal.* **2013**, *34*, 838−850.

(9) Chen, J.; Patil, S.; Seal, S.; McGinnis, J. F. Rare Earth Nanoparticles Prevent Retinal Degeneration Induced by Intracellular Peroxides. *Nat. Nanotechnol.* **2006**, *1*, 142−150.

(10) Basim, G. B.; Adler, J. J.; Mahajan, U.; Singh, R. K.; Moudgil, B. M. Effect of Particle Size of Chemical Mechanical Polishing Slurries for Enhanced Polishing with Minimal Defects. *J. Electrochem. Soc.* **2000**, *147*, 3523−3528.

(11) Harra, J.; Mäkitalo, J.; Siikanen, R.; Virkki, M.; Genty, G.; Kobayashi, T.; Kauranen, M.; Mäkelä, J. M. Size-Controlled Aerosol Synthesis of Silver Nanoparticles for Plasmonic Materials. *J. Nanoparticle Res.* **2012**, *14*, 870.

DOI: 10.1021/acsami.8b08674
ACS Appl. Mater. Interfaces 2018, 10, 32510−32515

(12) Sayle, T. X. T.; Cantoni, M.; Bhatta, U. M.; Parker, S. C.; Hall, S. R.; Möbus, G.; Molinari, M.; Reid, D.; Seal, S.; Sayle, D. C. Strain and Architecture-Tuned Reactivity in Ceria Nanostructures; Enhanced Catalytic Oxidation of CO to CO_2. *Chem. Mater.* **2012**, *24*, 1811−1821.
(13) Yao, H.; Yu Yao, Y. Ceria in automotive exhaust catalysts I. Oxygen storage. *J. Catal.* **1984**, *86*, 254−265.
(14) Xie, Z.; Liu, Z.; Wang, Y.; Yang, Q.; Xu, L.; Ding, W. An Overview of Recent Development in Composite Catalysts from Porous Materials for Various Reactions and Processes. *Int. J. Mol. Sci.* **2010**, *11*, 2152−2187.
(15) Sayle, T. X. T.; Kgatwane, K.; Ngoepe, P. E.; Sayle, D. C. "Breathing-crystals" the origin of electrochemical activity of mesoporous Li-MnO_2. *J. Mater. Chem. A* **2016**, *4*, 6456−6464.
(16) Crawford, G.; Chawla, N.; Das, K.; Bose, S.; Bandyopadhyay, A. Microstructure and deformation behavior of biocompatible TiO_2 nanotubes on titanium substrate☆. *Acta Biomater.* **2007**, *3*, 359−367.
(17) Eremets, M. I.; Trojan, I. A.; Gwaze, P.; Huth, J.; Boehler, R.; Blank, V. D. The Strength of Diamond. *Appl. Phys. Lett.* **2005**, *87*, 141902.
(18) Guillonneau, G.; Kermouche, G.; Bec, S.; Loubet, J.-L. Determination of Mechanical Properties by Nanoindentation Independently of Indentation Depth Measurement. *J. Mater. Res.* **2012**, *27*, 2551−2560.
(19) Badwal, S.; Ciacchi, F.; Drennan, J. Investigation of the stability of ceria-gadolinia electrolytes in solid oxide fuel cell environments. *Solid State Ionics* **1999**, *121*, 253−262.
(20) Deville, S.; El Attaoui, H.; Chevalier, J. Atomic Force Microscopy of Transformation Toughening in Ceria-Stabilized Zirconia. *J. Eur. Ceram. Soc.* **2005**, *25*, 3089−3096.
(21) Shokuhfar, T.; Arumugam, G. K.; Heiden, P. A.; Yassar, R. S.; Friedrich, C. Direct Compressive Measurements of Individual Titanium Dioxide Nanotubes. *ACS Nano* **2009**, *3*, 3098−3102.
(22) Caddeo, F.; Corrias, A.; Sayle, D. C. Tuning the Properties of Nanoceria by Applying Force: Stress-Induced Ostwald Ripening. *J. Phys. Chem. C* **2016**, *120*, 14337−14344.
(23) Sayle, T. X. T.; Inkson, B. J.; Möbus, G.; Parker, S. C.; Seal, S.; Sayle, D. C. Mechanical Properties of Mesoporous Ceria Nanoarchitectures. *Phys. Chem. Chem. Phys.* **2014**, *16*, 24899−24912.
(24) Sakanoi, R.; Shimazaki, T.; Xu, J.; Higuchi, Y.; Sato, K.; Hashida, T.; Kubo, M. Communication: Different behavior of Young's modulus and fracture strength of CeO_2: Density functional theory calculations. *J. Chem. Phys.* **2014**, *140*, 121102.
(25) Huang, Y.; Kawasaki, M.; Al-Zubaydi, A.; Langdon, T. G. Effect of Anvil Roughness on the Flow Patterns and Hardness Development in High-Pressure Torsion. *J. Mater. Sci.* **2014**, *49*, 6517−6528.
(26) Goel, S.; Haque Faisal, N.; Luo, X.; Yan, J.; Agrawal, A. Nanoindentation of Polysilicon and Single Crystal Silicon: Molecular Dynamics Simulation and Experimental Validation. *J. Phys. D: Appl. Phys.* **2014**, *47*, 275304.
(27) Lewis, G. V.; Catlow, C. R. A. Potential Models for Ionic Oxides. *J. Phys. C: Solid State Phys.* **1985**, *18*, 1149−1161.
(28) Sayle, T. X. T.; Catlow, C. R. A.; Maphanga, R. R.; Ngoepe, P. E.; Sayle, D. C. Generating MnO2Nanoparticles Using Simulated Amorphization and Recrystallization$_2$ Nanoparticles Using Simulated Amorphization and Recrystallization. *J. Am. Chem. Soc.* **2005**, *127*, 12828−12837.
(29) Sayle, T. X. T.; Inkson, B. J.; Karakoti, A.; Kumar, A.; Molinari, M.; Möbus, G.; Parker, S. C.; Seal, S.; Sayle, D. C. Mechanical Properties of Ceria Nanorods and Nanochains; the Effect of Dislocations, Grain-Boundaries and Oriented Attachment. *Nanoscale* **2011**, *3*, 1823−1837.
(30) Lin, Y.; Wu, Z.; Wen, J.; Poeppelmeier, K. R.; Marks, L. D. Imaging the Atomic Surface Structures of CeO2 Nanoparticles$_2$ Nanoparticles. *Nano Lett.* **2014**, *14*, 191−196.
(31) Skorodumova, N. V.; Hermansson, K.; Johansson, B. Structural and Electronic Properties of the (100) Surface and Bulk of Alkaline-Earth Metal Oxides. *Phys. Rev. B: Condens. Matter Mater. Phys.* **2005**, *72*, 125414.
(32) Gale, J. D.; Rohl, A. L. The General Utility Lattice Program (GULP). *Mol. Simul.* **2003**, *29*, 291−341.
(33) Todorov, I. T.; Smith, W.; Trachenko, K.; Dove, M. T. DL_POLY_3: New Dimensions in Molecular Dynamics Simulations via Massive Parallelism. *J. Mater. Chem.* **2006**, *16*, 1911−1918.
(34) Humphrey, W.; Dalke, A.; Schulten, K. VMD: Visual molecular dynamics. *J. Mol. Graphics* **1996**, *14*, 33−38.
(35) Mamontov, E.; Egami, T.; Brezny, R.; Koranne, M.; Tyagi, S. Lattice Defects and Oxygen Storage Capacity of Nanocrystalline Ceria and Ceria-Zirconia. *J. Phys. Chem. B* **2000**, *104*, 11110−11116.
(36) Fang, J.; Bull, C. L.; Loveday, J. S.; Nelmes, R. J.; Kamenev, K. V. Strength Analysis and Optimisation of Double-Toroidal Anvils for High-Pressure Research. *Rev. Sci. Instrum.* **2012**, *83*, 093902.
(37) Anders, C.; Bringa, E. M.; Ziegenhain, G.; Graham, G. A.; Hansen, J. F.; Park, N.; Teslich, N. E.; Urbassek, H. M. Why Nanoprojectiles Work Differently than Macroimpactors: The Role of Plastic Flow. *Phys. Rev. Lett.* **2012**, *108*, 027601.
(38) Li, Q.; Yu, Y.; Liu, Y.; Liu, C.; Lin, L. Thermal Properties of the Mixed n-Octadecane/Cu Nanoparticle Nanofluids during Phase Transition: A Molecular Dynamics Study. *Materials* **2017**, *10*, 38.
(39) Wang, Y.; Duncan, K.; Wachsman, E.; Ebrahimi, F. The effect of oxygen vacancy concentration on the elastic modulus of fluorite-structured oxides. *Solid State Ionics* **2007**, *178*, 53−58.
(40) Sato, K.; Yugami, H.; Hashida, T. Effect of Rare-Earth Oxides on Fracture Properties of Ceria Ceramics. *J. Mater. Sci.* **2004**, *39*, 5765−5770.
(41) Bhatta, U.; Briston, K.; Moebus, G.; Inkson, B. Multi-Cycle Rubbing of Ceria Nanoclusters: An In Situ TEM Study.
(42) Lockwood, A. J.; Inkson, B. J. In situ TEM nanoindentation and deformation of Si-nanoparticle clusters. *J. Phys. D: Appl. Phys.* **2009**, *42*, 035410.
(43) Epicier, T.; JolyPottuz, L.; Jenei, I.; Stauffer, D.; Dassenoy, F.; MasenelliVarlo, K. TEM Compression of NanoParticles in Environmental Mode and with Atomic Resolution Observations. *European Microscopy Congress 2016: Proceedings*, 2016.
(44) Podio-Guidugli, P.; Favata, A. *Elasticity for Geotechnicians*; Springer, 2013.
(45) Johnson, K. *Contact Mechanics*; Cambridge University Press, 1987.
(46) Gao, X.; Hao, F.; Fang, D.; Huang, Z. Boussinesq Problem with the Surface Effect and its Application to Contact Mechanics at the Nanoscale. *Int. J. Solid Struct.* **2013**, *50*, 2620−2630.

DOI: 10.1021/acsami.8b08674
ACS Appl. Mater. Interfaces 2018, 10, 32510−32515